Journal of Hazardous Materials 193 (2011) 243–248

Contents lists available at ScienceDirect

Journal of Hazardous Materials

journal homepage: www.elsevier.com/locate/jhazmat

Significant enhancement of the NO_2 sensing capability in networked SnO_2 nanowires by Au nanoparticles synthesized via γ-ray radiolysis

Sun-Woo Choi, Sung-Hyun Jung, Sang Sub Kim*

School of Materials Science and Engineering, Inha University, Incheon 402-751, Republic of Korea

ARTICLE INFO

Article history:
Received 2 April 2011
Received in revised form 13 July 2011
Accepted 14 July 2011
Available online 23 July 2011

Keywords:
Au nanoparticles
γ-Ray radiolysis
Functionalization
SnO_2 nanowires
Gas sensors

ABSTRACT

γ-Ray radiolysis was applied to the synthesis of Au nanoparticles. The growth behavior of Au nanoparticles was systematically investigated as a function of the processing parameters under γ-ray radiolysis. The surface of the networked SnO_2 nanowires fabricated through the vapor-phase selective growth process was uniformly functionalized with the Au nanoparticles by the γ-ray radiolysis process. Au nanoparticle-functionalized SnO_2 nanowires were compared to bare SnO_2 nanowires in terms of the NO_2 sensing characteristics. Au functionalization sharply improved the sensitivity and response time of SnO_2 nanowire-based gas sensors, most likely due to the spillover and the catalytic effects of Au nanoparticles. The methodology used in this work can be easily extended to synthesize various combinations of metal nanoparticles and oxide nanowires, which may be useful materials for use in detecting hazardous substances.

1. Introduction

Oxide nanowires have received an increasing amount of attention due to their unique physical and chemical properties, which are significantly different from those of their bulk or thin film counterparts. They have great potential for use as highly sensitive chemical gas sensors [1–5]. The extremely high surface-to-volume ratio and single crystallinity of oxide nanowires are why nanowire sensors are much more sensitive than those made from thin film or bulk materials.

In spite of the significant progress in fabricating chemical gas sensors using single nanowires, their practical application remains challenging due to the difficult fabrication process and the poor reproducibility [6]. In terms of the fabrication process and reliability, networked nanowire sensors exhibit good characteristics, apart from their decreased sensitivity and response time compared to single nanowire sensors. Therefore, improving these properties in networked nanowires is essential before these types of nanowires can be applied to chemical gas sensors.

Metallic catalysts are known to functionalize the surface of nanomaterials. For instance, noble metals anchored onto semiconducting oxides facilitate the dissociation of oxygen molecules into oxygen species, including atomic oxygen, thereby enhancing the oxygen sensitivity [7,8]. Various methods, such as photochemistry [9], reverse micelles [10], arc discharge [11], and sonochemistry [12] have been attempted to prepare metal nanoparticles. Radiolysis in which γ-rays are used has some advantages over such techniques, and thus a few research groups [13–16] have used γ-ray radiolysis for the preparation of metal nanoparticles. For example, Gachard et al. [13] prepared Au clusters and Henglein [14], Seino et al. [15], and Li et al. [16] synthesized Au nanoparticles using γ-ray radiolysis.

The addition of noble metals to SnO_2 nanowires is known to enhance gas sensitivity. Zhang et al. [17] prepared Au-decorated porous SnO_2 hollow spheres using an aqueous solution method that involved the application of $HAuCl_4$ as an Au precursor for the purpose of enhancing the sensitivity and selectivity of SnO_2-based sensors to detect ethanol. Qian et al. [18] synthesized a novel Au/SnO_2 nanostructure in which individual SnO_2 nanobelts were decorated by Au nanoparticles by means of conventional thermal evaporation. The Au-decorated SnO_2 nanobelt showed a 14-fold higher response to CO. Wang et al. [19] fabricated sensors consisting of Au/SnO_2 nanocrystals by a deposition-precipitation method. They investigated the CO sensing behavior of the sensors under different concentrations and tested the favorable effects of Au.

However, to the best of our knowledge, no work has reported Au-functionalization via γ-ray radiolysis on SnO_2 nanowires. In the present work, the growth of Au nanoparticles is investigated as a function of the processing parameters. Networked SnO_2 nanowires are prepared as a sensor platform and subsequently functionalized with Au nanoparticles via γ-ray radiolysis. The sensing characteristics of Au nanoparticle-functionalized SnO_2 nanowires as well as bare nanowires are studied in a comparative manner.

* Corresponding author. Tel.: +82 32 8607546; fax: +82 32 8625546.
E-mail address: sangsub@inha.ac.kr (S.S. Kim).

0304-3894/$ – see front matter © 2011 Elsevier B.V. All rights reserved.
doi:10.1016/j.jhazmat.2011.07.053

2. Experimental

2.1. Synthesis of Au nanoparticles by γ-ray radiolysis

For the radiolysis process, the precursor solutions were prepared as follows. Various contents ranging from 0.0496 to 0.496 mM of hydrogen tetrachloroaurate (III) hydrate ($HAuCl_4{\cdot}nH_2O$, $n = 3.5$, Kojima Chemicals Co.) were dissolved in a solvent of 2-propanol. The prepared solutions were stirred for 24 h, after which they were illuminated with ^{60}Co γ-rays under ambient air at room temperature at the Korea Atomic Energy Research Institute (KAERI).

For the purpose of investigating the growth behavior of Au nanoparticles by radiolysis systematically, the processing parameters of the precursor concentration, intensity, and exposure time of γ-ray illumination were varied while the other conditions were held constant. Si (1 0 0) wafers were used to support the Au nanoparticles synthesized in the solutions. For the functionalization of the surface of the networked SnO_2 nanowires, the fabricated sensor platforms were immersed into solutions of various precursor concentrations. The solutions were then illuminated by γ-rays. After γ-ray illumination, the samples were taken out from the solution container and heat-treated at 500 °C for 1 h in air to remove any remaining solvent.

2.2. Growth of networked SnO_2 nanowires

Networked SnO_2 nanowires were fabricated by the well-known vapor-phase selective growth method. For the selective growth of SnO_2 nanowires, patterned-interdigital electrodes (PIEs) were created on SiO_2-grown Si (1 0 0) substrates using a conventional photolithographic process. The electrodes were tri-layers consisting of Au (3 nm)/Pt (100 nm)/Ti (100 nm) that had sequentially been deposited by a sputtering method. A 100-nm-Ti layer was inserted between the SiO_2 and the Pt layers to improve the adhesion between them. The Au top layer served as a catalytic layer for selective growth.

The substrates on which the PIEs had been created were introduced into a horizontal quartz-tube furnace in which an alumina crucible containing Sn powders (Aldrich, 99.9%) was placed. The furnace was then evacuated by a rotary pump down to a pressure of 1×10^{-3} Torr and was heated to 900 °C for 15 min. During the vapor-phase growth of the SnO_2 nanowires, N_2 and O_2 flowed through the quartz tube at rates of 300 and 10 standard cubic centimeters per minute, respectively. The pressure of the tube furnace was maintained at 5 Torr.

The SnO_2 nanowires that were selectively grown on the PIEs became tangled with each other in the areas between the electrode spacings, consequently producing the networked junctions. 10-nm-spacing PIEs were used in this study. Fig. 1(a) and (b) shows plan- and the cross-section views, respectively, of the networked SnO_2 nanowires used for the sensor platforms in this study. The figures demonstrate the formation of the networked junctions.

2.3. Characterization and sensing

The microstructure of the synthesized Au nanoparticles was examined by field-emission scanning electron microscopy (FE-SEM, Hitachi, S-4200) and transmission electron microscopy (TEM, Philips CM-200), and the phase of the synthesized Au nanoparticles was examined by X-ray diffraction (XRD, Philips X'pert MRD diffractometer).

The response of the Au nanoparticle-functionalized networked SnO_2 nanowires to NO_2 was measured using a custom-made gas dilution and sensing system. The measurements were performed in a comparative manner versus the response of bare SnO_2 nanowires to NO_2 at various temperatures. The sensitivity (S) was estimated according to the formula $S = R_g/R_a$, where R_a is the resistance in the absence of NO_2 and R_g is the resistance measured in the presence of NO_2.

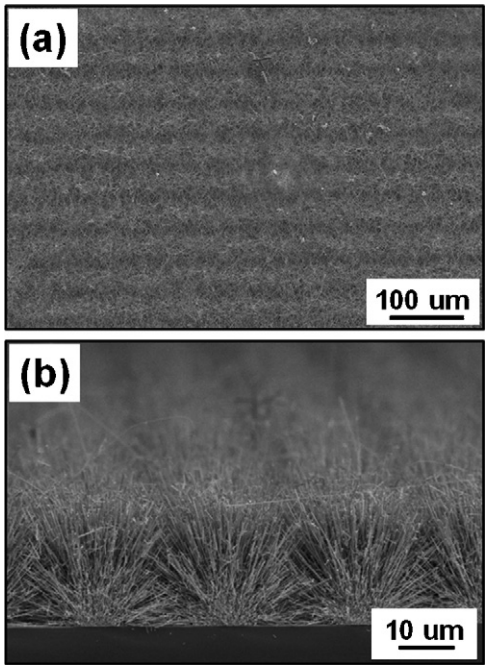

Fig. 1. Microstructures of networked SnO_2 nanowires grown on patterned electrode layers via vapor-phase selective growth: (a) plan and (b) cross-sectional views.

3. Results and discussion

The growth behavior of Au nanoparticles was investigated in relation to the radiolysis conditions. Fig. 2 shows typical FE-SEM images of Au nanoparticles synthesized with different precursor concentrations under 10 kGy h^{-1} γ-rays for 3 h. It is evident that Au nanoparticles of different sizes and densities are produced by the γ-ray radiolysis process. The average diameter and the formation density, that is, the number of nanoparticles per unit area, are summarized in Fig. 3. Lower concentrations of $HAuCl_4{\cdot}nH_2O$ produce smaller Au nanoparticles. The formation density is converse.

Fig. 4 shows the results for Au nanoparticles synthesized at various γ-ray intensities and exposure times: (a) various intensities for 2 h with 0.248 mM $HAuCl_4{\cdot}nH_2O$, and (b) various exposure times at 10 kGy h^{-1} with 0.248 m M $HAuCl_4{\cdot}nH_2O$. FE-SEM images of the samples are not displayed to avoid repetition. As clearly shown in Fig. 4, higher intensities lead to smaller Au nanoparticles. In addition, the Au nanoparticles gradually increase in size upon prolonged γ-ray exposure times. The formation density exhibits the reverse behavior with regard to the size of the nanoparticles.

The growth behavior of Au nanoparticles observed in this γ-ray radiolysis system can be explained as follows. At the initial stage of γ-ray radiolysis, electrons are likely to be generated by the water radiolysis process [20,21]. The electrons easily reduce the metal ions dissolved in the solutions because they act as strong reducing agents. The reduced neutral metal atoms encounter each other by diffusion, finally forming embryos. A further supply of reduced neutral metal atoms to the embryos creates metal nuclei that are thermodynamically stable. The nuclei grow and then coalesce at the expense of their smaller counterparts, eventually forming metal nanoparticles. At higher precursor concentrations, the production rate of neutral atoms increases, suggesting that more atoms diffuse into the nuclei, accordingly generating larger nanoparticles.

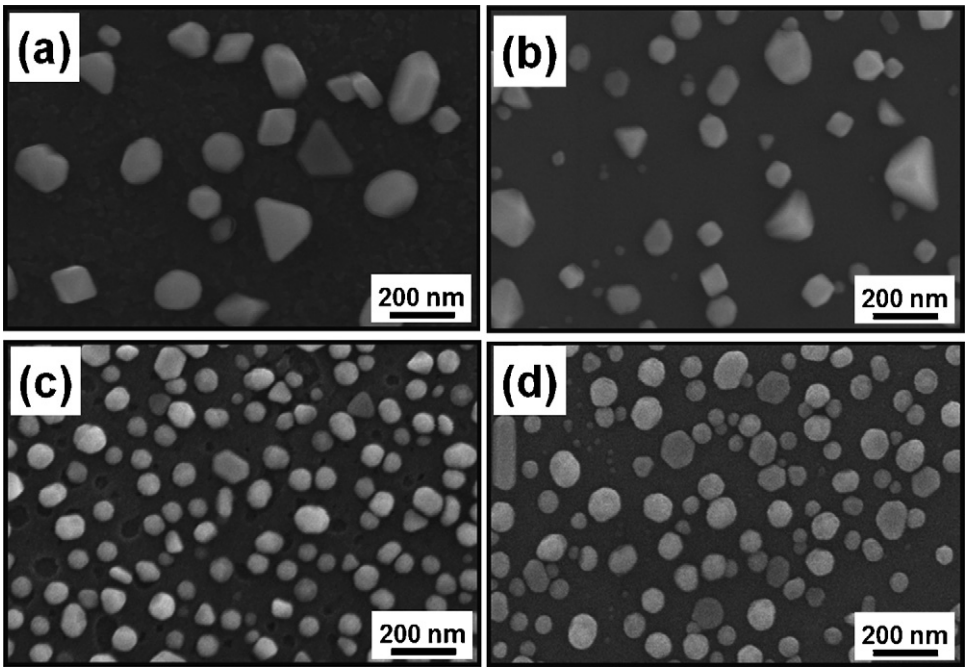

Fig. 2. Microstructures of Au nanoparticles synthesized with different $HAuCl_4{\cdot}nH_2O$ concentrations in γ-ray radiolysis at 10 kGy h^{-1} for 3 h: (a) 0.496, (b) 0.248, (c) 0.124, and (d) 0.0496 mM $HAuCl_4{\cdot}nH_2O$ in 2-propanol.

At a fixed precursor concentration, higher γ-ray intensities yield smaller nanoparticles, suggesting that a γ-ray intensity beyond a critical value is required to trigger the radiolysis reaction.

The microstructure of the Au nanoparticles was further investigated by TEM. Fig. 5(a) shows a typical TEM image taken from a sample synthesized under 10 kGy h^{-1} γ-rays with 0.248 mM $HAuCl_4{\cdot}nH_2O$ for 2 h. This figure shows round nanoparticles with diameters of approximately 60 nm. Fig. 5(b) is a high-resolution TEM image which highlights the single-crystalline nature of the individual Au nanoparticles. The interplanar spacing of 0.41 nm noted in the figure confirms the formation of Au.

On the networked SnO_2 nanowires, Au nanoparticles were synthesized using γ-ray radiolysis. Various γ-ray radiolysis conditions were applied. The results obtained from one set of experiments are shown in Fig. 6. This figure shows the morphologies of Au nanoparticle-functionalized SnO_2 nanowires under various γ-ray exposure times synthesized under 10 kGy h^{-1} γ-rays with 0.248 mM $HAuCl_4{\cdot}nH_2O$. The FE-SEM images clearly show that nanoparticles in the range of 10–80 nm in diameter are homogeneously distributed on the surfaces of individual SnO_2 nanowires. It is also evident that one can obtain a target size and formation density of Au nanoparticles on SnO_2 nanowires by changing the γ-ray radiolysis conditions.

The microstructure of Au nanoparticles on SnO_2 nanowires was further investigated by TEM. Fig. 7(a) and (b) respectively shows low- and high-magnification TEM images that were taken of Au nanoparticle-functionalized SnO_2 nanowires synthesized under the following conditions: 0.248 mM $HAuCl_4{\cdot}nH_2O$, 10 kGy h^{-1}, and

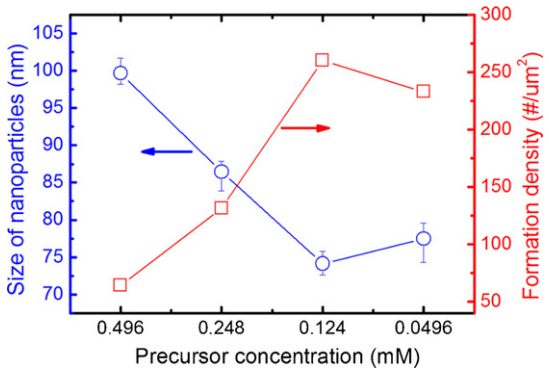

Fig. 3. Size and formation density of Au nanoparticles with respect to the precursor concentration in γ-ray radiolysis at 10 kGy h^{-1} for 3 h.

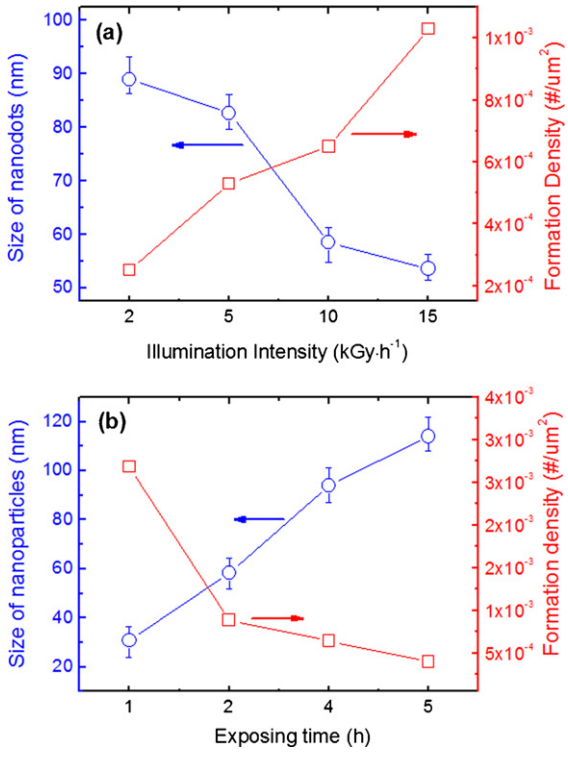

Fig. 4. Size and formation density of Au nanoparticles with respect to (a) the illumination intensity during γ-ray radiolysis at 0.248 mM $HAuCl_4{\cdot}nH_2O$ for 2 h, and (b) the exposure time at10 kGy h^{-1} and 0.248 mM $HAuCl_4{\cdot}nH_2O$.

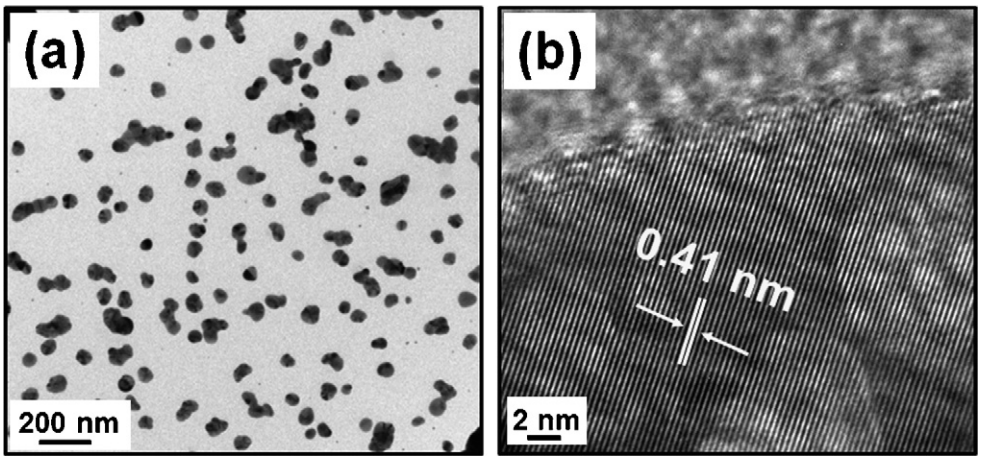

Fig. 5. (a) Typical TEM image and (b) lattice image taken of Au nanoparticles synthesized at 10 kGy h^{-1} and 0.248 mM for 2 h.

a 2 h exposure time. As clearly shown in Fig. 7(a), Au nanoparticles appear uniformly distributed and well anchored onto the surface of the SnO_2 nanowire. The high-resolution TEM image in Fig. 7(b) shows the lattice fringes of the SnO_2 nanowire and the Au nanoparticles. The clear interface between the SnO_2 nanowire and the Au nanoparticles indicates that no significant reaction occurs during the γ-ray radiolysis process.

The sensing properties of the networked SnO_2 nanowires that had been functionalized with Au nanoparticles were compared to those of bare SnO_2 nanowires in terms of their capability to sense NO_2. In the case of bare SnO_2 nanowires, as shown in Fig. 8(a), the resistance increases/decreases slowly with the supply/cutoff of 30 ppm NO_2. In contrast, the resistance of the Au nanoparticle-functionalized SnO_2 nanowires increases and decreases more

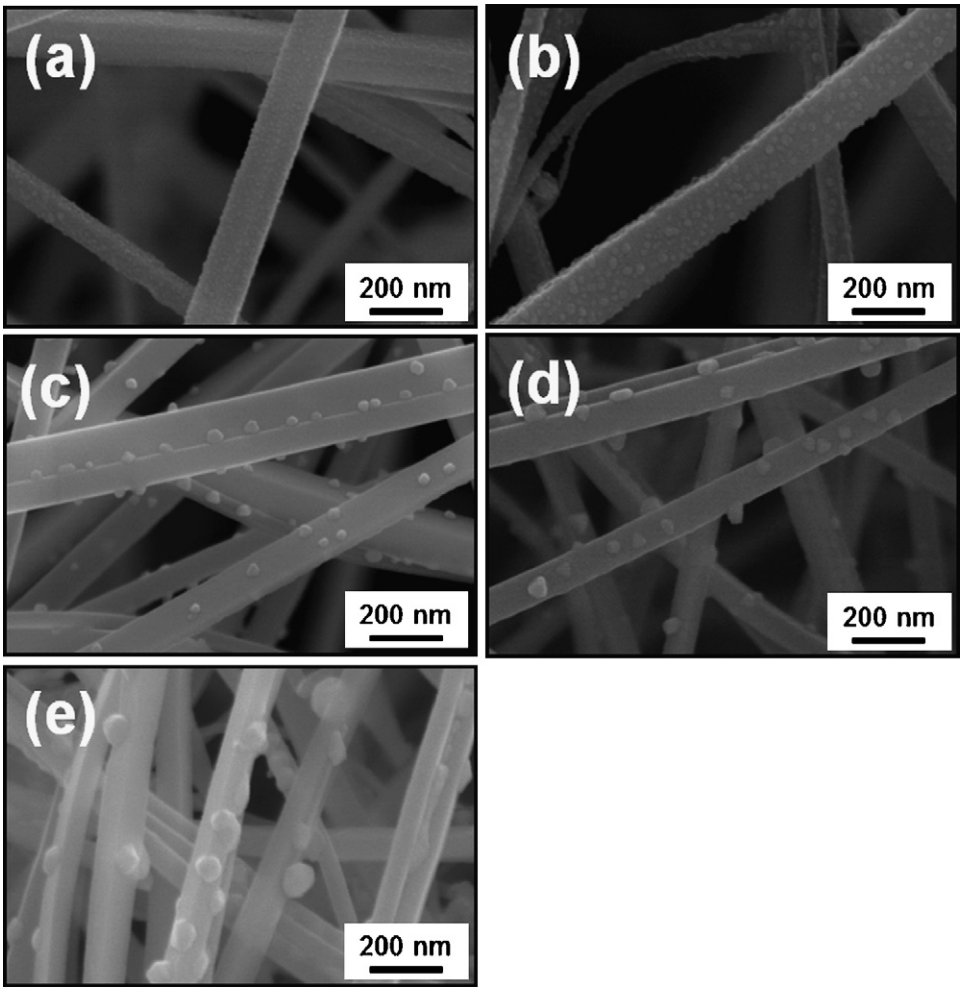

Fig. 6. Microstructures of Au nanoparticle-functionalized SnO_2 nanowires via γ-ray radiolysis: Exposure time: (a) 1, (b) 2, (c) 3, (d) 4 h, and (e) 5 h at 10 kGy h^{-1} and 0.248 mM $HAuCl_4 \cdot nH_2O$.

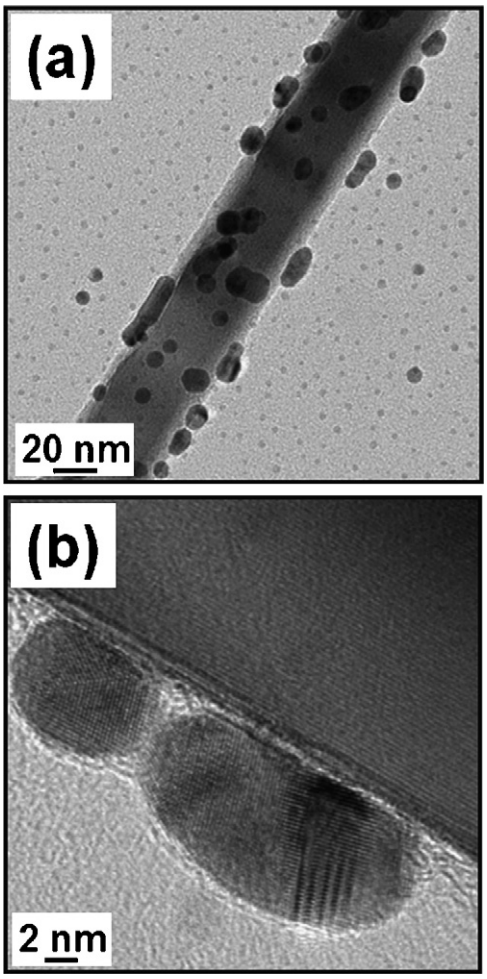

Fig. 7. (a) Low- and (b) high-magnification TEM images taken from an SnO_2 nanowire functionalized with Au nanoparticles under the following conditions: 0.248 mM $HAuCl_4 \cdot nH_2O$, 10 kGy h^{-1}, and 2 h.

rapidly. The change in the resistance of the sensors can be explained via the framework of the n-type semiconductors. The resistance increases upon exposure to NO_2, whereas it decreases upon the removal of NO_2. NO_2 molecules adsorbed on the surface of the networked SnO_2 nanowires are likely to extract electrons from the nanowires, eventually leading to the surface depletion of each SnO_2 nanowire. On the other hand, a release of electrons occurs in conjunction with the desorption of the NO_2 molecules. This charge transfer accounts for the resistance change observed in the sensors. Importantly, a remarkable difference in the shape of the transient response was introduced by the Au-functionalization process. The response times, defined as the time to reach 90% of the final value of resistance, of the sensors fabricated from the bare and the Au-functionalized SnO_2 nanowires were 470 and 35 s, respectively. The sensitivities measured at different NO_2 concentrations are summarized in Fig. 8(b). No meaningful results were obtained below 30 ppm NO_2 for the bare SnO_2 nanowires. The sensitivity of the Au-functionalized SnO_2 nanowires is higher by a factor of ~33 for >30 ppm NO_2. The Au-functionalized SnO_2 nanowires were tested at various temperatures ranging from 50 to 300 °C to evaluate their performance as NO_2 gas sensors. The results obtained at 200 °C are presented in Fig. 9(a). For clarity, the inset in Fig. 9(a) is an enlargement of the result obtained at 0.1 ppm NO_2.

It should also be noted here that the density and size of the Au nanoparticles greatly influenced the NO_2 sensing capability. Detailed results pertaining to this will be reported at a later time.

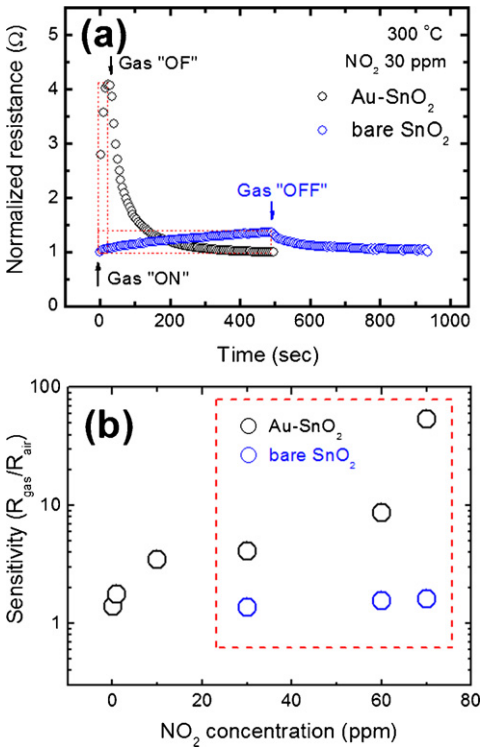

Fig. 8. (a) Response curves of sensors fabricated with bare networked SnO_2 nanowires and with Au-functionalized networked SnO_2 nanowires to 30 ppm NO_2 at 300 °C. (b) Sensitivity as a function of NO_2 measured at 300 °C.

To estimate the quality of the Au-functionalized SnO_2 nanowire sensor, its sensitivity is compared to a range of reported values [17,19,22,23] in Fig. 10. Regardless of the measuring gas temperature, it is reasonable to conclude that the Au-functionalized SnO_2 nanowires fabricated in this work are of high quality.

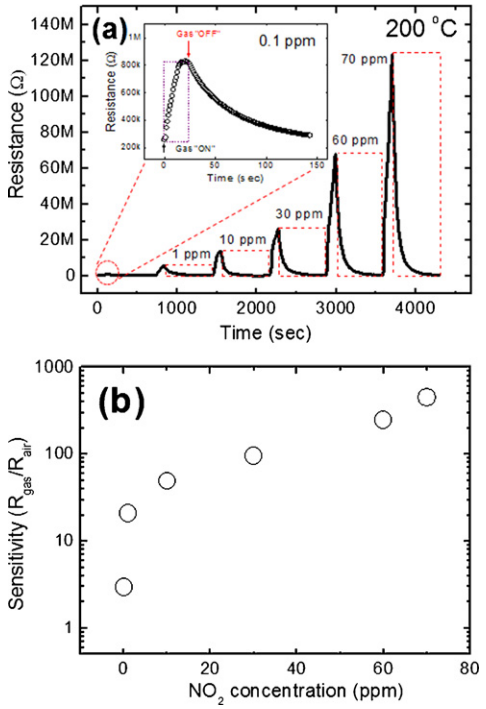

Fig. 9. (a) Response curves and (b) summary of the sensitivity of the Au-functionalized networked SnO_2 nanowires at 200 °C.

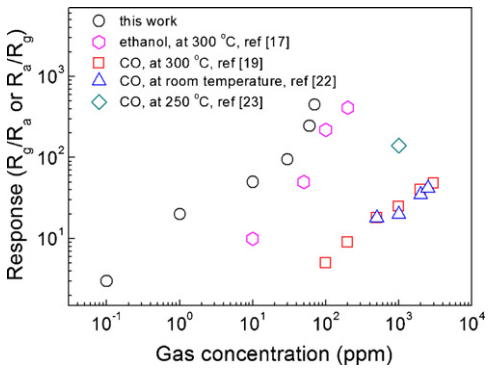

Fig. 10. The sensitivity of a sensor fabricated with Au nanoparticle-functionalized SnO_2 nanowires in this work is compared to those of previously reported Au-SnO_2 gas sensors fabricated with different types of Au and SnO_2 materials.

There are several possible reasons for this gas-sensing enhancement by Au nanoparticles. One possibility is that the Au nanoparticles attached to the SnO_2 nanowires provide more active sites for NO_2 adsorption through a process known as the spillover effect [24]. In the case of the Au-functionalized SnO_2 nanowires, NO_2 is easily adsorbed onto the Au nanoparticles and migrates onto the SnO_2 nanowires, which are less likely to be adsorbed by NO_2. Accordingly, by means of the NO_2-spillover effect, the adsorption of the NO_2 species is facilitated. Hence, the size of the depletion layer can grow even more, with the underlying conduction channel being suppressed further. The increased reduction of the conductance corresponds to the enhancement of NO_2 sensitivity. Moreover, as sufficient sensitivity can be attained even with a small amount of NO_2 gas, the Au-functionalization process can accelerate the response time. Another possibility is that the Au nanoparticles facilitate the dissociation of NO_2 into ionized or neutral chemical species, possibly including NO, O, NO_2^-, NO^+, and NO^- [25–27]. These dissociated chemical species readily capture the electrons in SnO_2 nanowires, indicating the intensification of the sensing signal with respect to NO_2 gas.

4. Conclusion

Au nanoparticles were synthesized by a γ-ray radiolysis process. The size and formation density of the Au nanoparticles were highly influenced by the processing parameters. A longer exposure time, lower γ-ray intensity, and higher precursor concentration led to larger Au nanoparticles but a lower formation density. Using γ-ray radiolysis, Au nanoparticles were successfully grown and anchored onto the surface of networked SnO_2 nanowires. In an NO_2 gas-sensing test, the Au-functionalized SnO_2 nanowires exhibited greatly superior sensitivity and faster response times compared to bare SnO_2 nanowires.

Acknowledgments

This work was supported by the Nuclear R&D program through the National Research Foundation of Korea.

References

[1] G. Yu, A. Cao, C.M. Lieber, Large-area blown bubble films of aligned nanowires and carbon nanotube , Nat. Nanotechnol. 2 (2007) 372–377.
[2] M. Kaur, N. Jain, K. Sharma, S. Bhattacharya, M. Roy, A.K. Tyagi, S.K. Gupta, J.V. Yakhmi, Room-temperature H_2S gas sensing at ppb level by single crystal In_2O_3 whiskers , Sens. Actuators B 133 (2008) 456–461.
[3] J. Chen, K. Wang, L. Hartman, W. Zhou, H_2S detection by vertically aligned CuO nanowire array sensors , J. Phys. Chem. C 112 (2008) 16017–16021.
[4] H.S. Kim, S.E. Park, H.W. Kim, J.Y. Park, N. Jiang, S.S. Kim, Fabrication of metal-shelled coaxial nanowires and annealing-induced formation of metal nanoparticles for catalytic applications: growth and characteristics of SnO_2-branched nanostructures , Solid State Sci. 12 (2010) 970–977.
[5] Q.-H. Wu, J. Li, S.-G. Sun, Nano SnO_2 gas sensors , Curr. Nanosci. 6 (2010) 525–535.
[6] J.Y. Park, D.E. Song, S.S. Kim, An approach to fabricating chemical sensors based on ZnO nanorod arrays , Nanotechnology 19 (2008) 105503.
[7] B. Chwieroth, B.R. Patton, Y. Wang, Conduction and gas-surface reaction modeling in metal oxide gas sensors , J. Electroceram. 6 (2001) 27.
[8] S.S. Kim, J.Y. Park, S.-W. Choi, H.S. Kim, H.G. Na, J.C. Yang, H.W. Kim, Significant enhancement of the sensing characteristics of In_2O_3 nanowires by functionalization with Pt nanoparticles , Nanotechnology 21 (2010) 415502.
[9] S. Kundu, S. Panigrahi, S. Pragaraj, S. Basu, S.K. Ghosh, A. Pal, T. Pal, Aninsotropic growth of gold clusters to gold nanocubes under UV irradiation , Nanotechnology 18 (2007) 075712.
[10] L.B. Scaffardi, N. Pellegri, O. de Sanceis, J.O. Tocho, Sizing gold nanoparticles by optical extinction spectroscopy , Nanotechnology 16 (2005) 158–163.
[11] J.-K. Lung, J.-C. Huang, D.-C. Tien, C.-Y. Liao, K.-H. Tseng, T.-T. Tsung, W.-S. Kao, T.-H. Tasi, C.-S. Jwo, H.-M. Lin, L. Stobinski, Preparation of gold nanoparticles by arc discharge in water , J. Alloys Compd. 434 (2007) 655–658.
[12] Y. Mizukoshi, S. Seino, K. Okitsu, T. Kinoshita, Y. Otome, T. Nakagawa, T.A. Yamamoto, Sonochemical preparation of composite nanoparticles of Au/γ-Fe_2O_3 and magnetic separation of glutathione , Ultrason. Sonochem. 12 (2001) 191–195.
[13] E. Gachard, H. Remita, J. Khatouri, B. Keita, L. Nadjo, J. Belloni, Radiation-induced and chemical formation of gold clusters , New J. Chem. 22 (1998) 1257–1265.
[14] A. Henglein, Radiolytic preparation of ultrafine colloidal gold particles in aqueous solution: optical spectrum, controlled growth, and some chemical reactions , Langmuir 15 (1999) 6738–6744.
[15] S. Seino, T. Kinoshita, Y. Otome, T. Maki, T. Nakagawa, K. Okitsu, Y. Mizukoshi, T. Nakarama, T. Sekino, K. Niihara, T.A. Yamamoto, γ-Ray synthesis of composite nanoparticles of noble metals and magnetic iron oxides , Scripta Mater. 51 (2004) 467–472.
[16] T. Li, H.G. Park, S.-H. Choi, γ-Irradiation-induced preparation of Ag and Au nanoparticles and their characterizations , Mater. Chem. Phys. 105 (2007) 325–330.
[17] J. Zhang, X. Liu, S. Wu, M. Xu, X. Guo, S. Wang, Au nanoparticle-decorated porous SnO_2 hollow sphere: a new model for a chemical sensor , J. Mater. Chem. 20 (2010) 6453–6459.
[18] L.H. Qian, K. Wang, H.T. Fang, Y. Li, X.L. Ma, Au nanoparticles enhance CO oxidation onto SnO_2 nanobelt , Mater. Chem. Phys. 103 (2007) 132–136.
[19] S. Wang, Y. Zhao, J. Huang, Y. Wang, S. Wu, S. Zhang, W. Huang, Low-temperature carbon monoxide gas sensors based gold/tin dioxide , Solid-State Electon. 50 (2006) 1728–1731.
[20] G. Ershov, A. Henglein, Optical spectrum and some chemical properties of colloidal thallium in aqueous solution , J. Phys. Chem. 97 (1993) 3434–3436.
[21] J. Belloni, Nucleation, growth and properties of nanoclusters studied by radiation chemistry application to catalysis , Catal. Today 113 (2006) 141–156.
[22] N. Du, H. Zhang, X. Ma, D. Yang, Homogenous coating of Au and SnO_2 nancrystals on carbon nanotubes via layer-by-layer assembly: a new ternary hybrid for a room-temperature CO gas sensor , Chem. Commun. (2008) 6182–6184.
[23] B. Bahrami, A. Khodadadi, M. Kazemeini, Y. Mortazavi, Enhanced CO sensitivity and selectivity of gold nanoparticles-doped SnO_2 sensor in presence of propane and methane , Sens. Actuators B 133 (2008) 352–356.
[24] A. Kolmakov, D.O. Klenov, Y. Lilac, S. Stemmer, M. Moskovits, Enhanced gas sensing by individual SnO_2 nanowires and nanobelts functionalized with Pd catalyst particles , Nano Lett. 5 (2005) 667–673.
[25] J. Tamaki, M. Nagaishi, Y. Teraoka, N. Miura, N. Yamazoe, Adsorption behavior of CO and interfering gases on SnO_2 , Surf. Sci. 2221 (1989) 183–196.
[26] B. Ruhland, Th. Becker, G. Müller, Gas-kinetic interactions of nitrous oxides with SnO_2 surfaces , Sens. Actuators B 50 (1998) 85–94.
[27] S.-H. Wang, T.-C. Chou, C.-C. Liu, Nano-crystalline tungsten oxide NO_2 sensor , Sens. Actuators B 94 (2003) 343–351.